Pattern selection in the generalized Swift-Hohenberg model

M' F. Hilali, S. Métens, P. Borckmans, and G. Dewel

Service de Chimie-Physique and Centre for Nonlinear Phenomena and Complex Systems,
Université Libre de Bruxelles, Code Postal 231, 1050 Brussels, Belgium

The competition between patterns of different symmetries is studied for the generalized Swift-Hohenberg model in the presence of a large quadratic coupling in one dimension (1D) and 2D. It is shown that hexagons with different phase relations may coexist for some values of the control parameter. Numerical experiments exhibiting the effects of linear spatial ramps of the control parameter on this selection are presented. The analogy with recent patterns obtained experimentally in open chemical reactors is also discussed.

PACS number(s): 47.54.+r, 82.40.Ck

I. INTRODUCTION

Symmetry-breaking instabilities giving rise to spatial patterns in driven systems have been the focus of great activity [1] in fields as diverse as hydrodynamics of simple fluids or liquid crystals, chemistry, and nonlinear optics [2–4].

From a theoretical point of view the nonlinear partial differential equations describing these systems cannot be solved exactly for most realistic conditions. A qualitative approach has therefore been developed based on simple models, which nevertheless can capture various experimental observations made in different systems. Such models are then able to provide an understanding of the basic underlying mechanisms. The need for such a metaphoric approach is particularly important in the chemical context, where the systems of interest generally involve a great number of species and for which the details of the corresponding kinetic mechanisms are generally largely unresolved.

In this framework the so-called generalized Swift-Hohenberg (GSH) model [5,6] provides a useful tool to analyze the competition between structures of hexagonal symmetry and patterns periodic in one direction, "rolls" or "stripes" [7], as well as the dynamics of their topological defects [8]. It takes the following form:

$$\frac{\partial u}{\partial t} = ru - [\nabla^2 + q_c^2]^2 u + vu^2 - gu^3 \quad (g > 0) , \tag{1}$$

where r is the bifurcation parameter. This equation has been widely used for a qualitative description of convective structures induced by the Bénard-Marangoni instability or non-Boussinesq Bénard convection [7,9]. In the latter case the quadratic term v is small since it is related to the terms associated, for instance, with the weak temperature dependence of the transport coefficients.

Such a model also proves useful to describe the Turing structures [10] that can appear through diffusion driven instabilities in chemical systems [11], and which have recently been obtained experimentally with the chlorite-iodide-malonic acid (CIMA) reaction in open gel reactors [12,13]. In these systems the quadratic term v, which can

be expressed in terms of the rate and diffusion constants, is however *not* necessarily *small*.

Although further generalizations of the SH model have recently been analyzed [14,15], the main purpose of this paper is to present aspects of the bifurcation analysis of the "simple" Eq. (1), when however v is not small but nevertheless such that $r_L = q_c^4 - v^2/4g$ remains positive in contrast to Ref. [9]. We show that this system exhibits a surprisingly rich nonlinear phenomenology that had not been made explicit previously, and that is due to the existence of reentrant hexagonal modes and localized structures.

The bifurcation diagrams are computed from the patterns obtained by integrating Eq. (1) with either no flux or mixed boundary conditions (periodic along one direction and no flux along the other in order to be able to introduce some ramps of the control parameter). They are discussed with the help of the relevant amplitude equations derived through the standard bifurcation analysis techniques. Furthermore in the presence of a spatial ramp of the control parameter r that mimics the feeding of the chemical reactor through its boundaries, the competition between these structures then gives rise to scenarios that are qualitatively analogous to those observed in open gel reactors.

II. THE MODEL: BASIC PROPERTIES

Let us briefly recall that Eq. (1) may be written in a gradient form

$$\frac{\partial u}{\partial t} = -\frac{\delta F}{\delta u} , \tag{2}$$

where F is a Lyapunov functional

$$F = \frac{1}{2} \int d\mathbf{x} \{ -ru^2 - \frac{2}{3}vu^3 + \frac{1}{2}gu^4 + [(\nabla^2 + q_c^2)u]^2 \} \tag{3}$$

that decreases along any trajectory during the evolution of the system:

$$\frac{\partial F}{\partial t} = -\int d\mathbf{x} \left[\frac{\partial u}{\partial t} \right]^2 \leq 0 , \tag{4}$$

where **x** is the D-dimensional position vector. This gradient property implies that only static attractors may appear, and its existence allows the relative stability of the various states to be computed. Hence the absolute minimum of F corresponds to the stable steady state, whereas the relative minima point to metastability. All this, however, does not preclude the onset of spatial disorder resulting from the multistability of states [9], as we will discuss below.

The homogeneous steady states are given by the solutions of

$$(r - q_c^4)u_s + vu_s^2 - gu_s^3 = 0 \ . \tag{5}$$

The reference state $u_0 = 0$ undergoes a transcritical bifurcation at $r = q_c^4$, leading to new branches, $u_\pm$, of uniform solutions (Fig. 1):

$$u_\pm = \frac{1}{2g}\{v \pm [v^2 + 4g(r - q_c^4)]^{1/2}\} \ . \tag{6}$$

At the limit point B, $r = r_L = q_c^4 - v^2/4g$, the stable (u_+) and unstable (u_-) branches annihilate. Bistability between uniform states $u = u_0 = 0$ and $u = u_+$ occurs for $r_L \leq r \leq q_c^4$.

In modeling convective flows by the Swift-Hohenberg models, u_0 corresponds to the conductive solution. There, the control parameter r is usually considered to be much smaller than q_c^4. As v is then also taken to be zero or small (Boussinesq or non-Boussinesq fluids, respectively), the uniform states $u_\pm$ lie generally far from the symmetry-breaking (convection) threshold $r = 0$ and are considered spurious.

On the contrary, in well-mixed open reactor conditions, i.e., in the absence of spatial contributions, the CIMA reaction can exhibit bistability between two uniform steady states, one reduced and the other oxidized [16]. Equation (1) thus provides a simple model to study t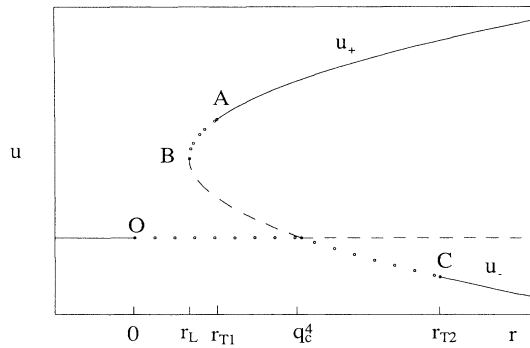he onset of patterned fronts between two steady states in asymmetrically fed unstirred reactors, as its steady solutions can be destabilized by inhomogeneous perturbations of wave vectors q_c.

The model, Eq. (1), indeed exhibits three pattern forming instabilities at points O $(r = 0)$, A $(r = r_{T1})$, and C $(r = r_{T2})$ that would be related to Turing instabilities in the chemical context. Figure 1 represents the uniform steady states (u_0, u_+, u_-) and their symmetry-breaking instabilities that can easily be computed by testing the stability of the uniform branches to space dependant perturbations. The values of the parameters $q_c = 0.5$, $v = 0.41$, and $g = 1$ used in this paper are chosen in order to dispose of a high value of the quadratic coupling v, while avoiding both the interaction of the symmetry-breaking bifurcation at A $(r = r_{T1})$ with the saddle-node bifurcation at B $(r = r_L)$, or the situation where the limit point B lies in the region $r < 0$ that has partly been analyzed elsewhere and that would occur for still larger values of v [9]. We will now study, analytically and numerically, the various spatial branches emerging from these points and show that they lead to a complex bifurcation diagram already for 1D systems.

III. 1D SYSTEM: SUBCRITICAL TRANSITIONS TO PERIODIC STRUCTURES

In the vicinity of each of the above mentioned symmetry-breaking instability points, the GSH model dynamics may be described in terms of an equation for the complex amplitude A of the pattern that plays the role of an order parameter [17]. We will here restrict our discussion of the pattern selection to the competition between solutions of different symmetry. Spatial modulations of the amplitudes will thus be neglected.

Near point O $(r = 0)$, at the lowest order, one finds

$$\frac{dA}{dt} = rA - g_3|A|^2A \ , \tag{7}$$

with

$$g_3 = 3g - \frac{38v^2}{9q_c^4} \ . \tag{8}$$

When the quadratic coupling coefficient v is small, g_3 is positive, and Eq. (7) describes the standard supercritical bifurcation at $r = 0$ of a 1D periodic structure: stripes.

On the other hand, when v becomes sufficiently large—and this is often the case for chemical systems, as we have already stated—g_3 may become negative and the amplitude can no longer be saturated by the cubic term. The value of v we have chosen corresponds to such a case. Higher order contributions must then be taken into account. Up to fifth order, near $r = 0$, the amplitude equation then takes the form [18]

$$\frac{dA}{dt} = rA - g_3|A|^2A - g_5|A|^4A \ , \tag{9}$$

with

$$g_3 = 3g - \frac{38v^2}{9q_c^4} - \frac{326rv^2}{81q_c^8} - \frac{2918r^2v^2}{729q_c^{12}} \ , \tag{10}$$

FIG. 1. Bifurcation diagram exhibiting the stability of the uniform states for $q_c = 0.5$, $g = 1$, $v = 0.41$. The same values of the parameters are used throughout the paper. The plain, dashed, and circled lines, respectively, correspond to linearly stable steady states, steady states already unstable to uniform perturbations, and those unstable with respect to the space dependent perturbations because of the presence of the O, A, and C symmetry-breaking bifurcations.
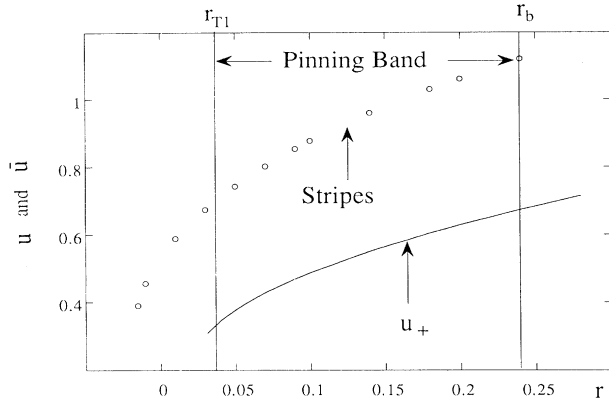
FIG. 2. Bifurcation diagram in one space dimension obtained from the numerical integration of Eq. (1). The amplitude u of the uniform u_+ state, and $\bar{u}$, the peak-to-peak amplitude of the striped structures, are represented.

$$g_5 = -\frac{3g^2}{64q_c^4} + \frac{13\,903v^2g}{864q_c^8} + \frac{301\,349v^4}{11\,664q_c^{12}} \ . \tag{11}$$

Since $g_3 < 0$ and $g_5 > 0$ for the values of the parameters chosen in our simulations, the resulting stripe structure indeed appears subcritically in the vicinity of $r = 0$ through an inverted pitchfork bifurcation. The subcritical nature of the bifurcation may be verified through numerical integration of Eq. (1).

Numerical simulations show (Fig. 2) that this branch of stripes develops with increasing amplitude until $r = r_b$. At higher values of r only the uniform u_+ states remain stable. Because no other structures are revealed numerically when $0 < r < r_{T1}$, it is reasonable to assume that at r_b the branches of periodic structures annihilate with the unstable branches emanating from subcritical structure forming bifurcations at $r = r_{T1}$ or r_{T2} on u_+. This may also be checked by deriving the amplitude equations near $r = r_{T1}$ or r_{T2}.

The system thus exhibits two successive regions of bistability:

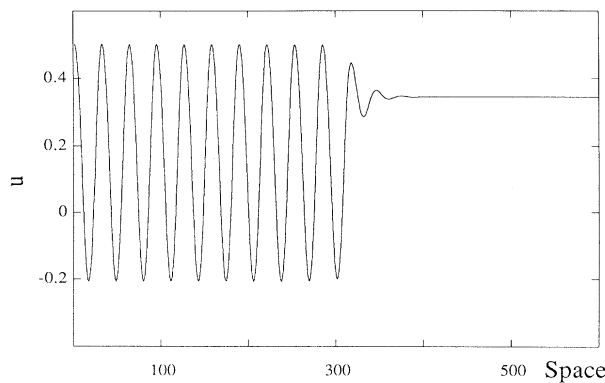(i) Between the stripes and the reference state ($A = 0$)

FIG. 3. Pinned (immobile) 1D front separating a striped 1D structure from the u_+ uniform steady state that coexist in space for $r = 0.1$.
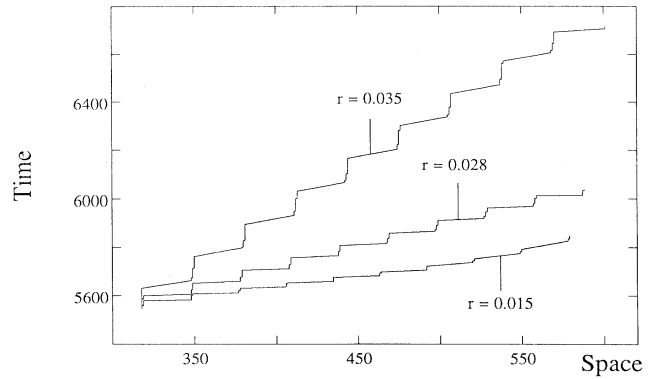

FIG. 4. Evolution in time of the position of a 1D front that was pinned at time $t = 0$ near the center of the system (position 300) in the pinning band for $r = 0.1$. The control parameter is then lowered, respectively, to $r = 0.035$, $r = 0.028$, and $r = 0.015$, values that are increasingly distant from the lower boundary ($r \approx 0.0375$) of the pinning region. The structure invades the domain of the u_+ uniform state with a nonuniform velocity. The movement proceeds by "jumps" of one wavelength of the structure. The time between each jump increases, while the mean velocity of the front decreases as the bifurcation parameter grows towards the pinning band edge. At this edge the time between jumps diverges so that pinning occurs.
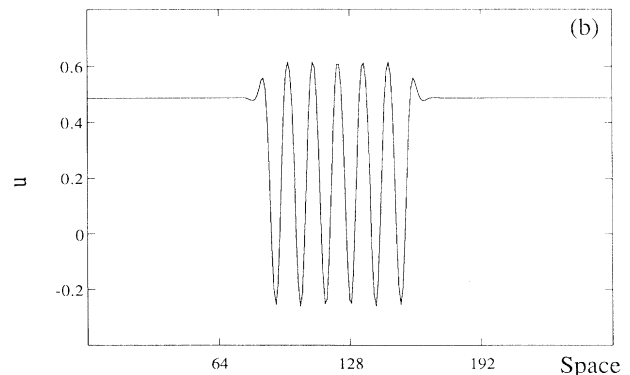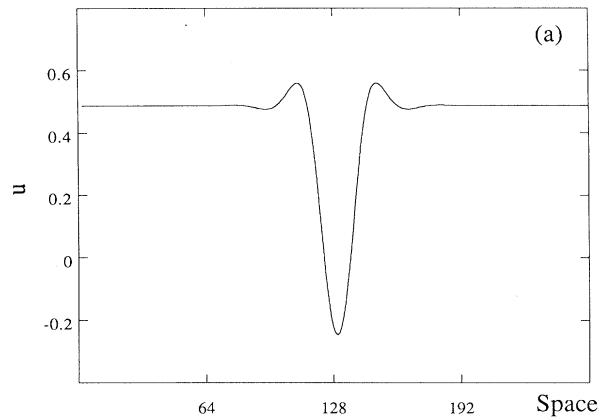

FIG. 5. 1D localized structures between the uniform u_+ state and 1D stripes obtained numerically from Eq. (1) at $r = 0.1$. (a) simple core; (b) multiple wavelengths core.

for $-g_3^2/4g_5 < r < 0$, and (ii) between the stripes and the states $u_{\pm}$ for $r_{T1,2} < r < r_b$.

Unsurprisingly, in these regions of bistability, stable stationary *localized* structures have been found numerically. The simplest correspond to *fronts (kinks)* that interconnect in space the two bistable states. An example of such a front, in the second region defined above, is shown in Fig. 3. Because the GSH model has a gradient structure, the stabilizing mechanism for this coherent structure is here provided by the pinning of the front by the periodic pattern [19]. Such nonadiabatic effects, as they have been coined, that cannot be accounted for by the amplitude equations [Eq. (8) or (10)], have also recently been observed [20] in a realistic chemical model. For the parameters considered, the pinning force appears to be large, as the pinning band covers nearly the whole domain of bistability between the $u_{\pm}$ uniform states and the stripes. As a consequence, propagating fronts between these two states can only be observed in a very narrow region near the stability limits r_{T1} (or r_{T2}) and r_b. Outside, but near the band edge, the front exhibits the stepwise motion, characterizing the nearby existence of pinning, with the typical critical slowing down of the mean velocity of the front as one comes close to the edges (Fig. 4).

Such fronts may then serve, and this is corroborated by our simulations, as building blocks for the construction of localized Turing structures embedded in an otherwise uniform background where the system is in a uniform state. The pinning effects are then also responsible for the observed multistability between localized states with different numbers of wavelengths in the core (Fig. 5).

For the values of the parameters used in the present simulations, the droplets present spatial oscillating tails. This gives rise to an effective potential between localized states that is a periodic function of the distance between them. As in condensed matter physics, such a potential provides a key ingredient for the onset of frozen-in disorder, even in gradient systems [21].

IV. 2D SYSTEM: PERIODIC AND LOCALIZED STRUCTURES

In 2D, besides the stripes, we also have to take into account structures built on a triad of active modes characterized by three pairs of wave vectors that are such that $\mathbf{q}_i \cdot \mathbf{q}_j = q_c^2 \cos 2\pi/3$ $(i, j = 1, 2, 3)$. These generate, as is well known, patterns with hexagonal symmetry.

When deriving the amplitude equations for three resonant pairs of active modes, we notice that, for our choice of parameters, the cubic nonlinearity does not saturate the instability. Therefore, as previously done for the stripes, we have to include higher order contributions. Using the same techniques [17], we obtain

$$\frac{dA_1}{dt} = rA_1 + 2vA_2^*A_3^* - g_3|A_1|^2A_1 - h_3[|A_2|^2 + |A_3|^2]A_1 - 2v'A_2^*A_3^*|A_1|^2 - v'A_2^*A_3^*[|A_2|^2 + |A_3|^2]$$

$$- v'A_1^2A_2A_3 - g_5|A_1|^4A_1 - h_5[|A_2|^4 + |A_3|^4]A_1 - h_5'[|A_2|^2 + |A_3|^2]|A_1|^2A_1$$

$$- h_5''[|A_2|^2|A_3|^2]A_1 - wA_1^*A_2^{*2}A_3^{*2} \tag{12}$$

and permutations thereof for A_2 and A_3. The various coefficients are given by

$$h_3 = 6g - \frac{5v^2}{q_c^4} - \frac{17v^2r}{4q_c^8} - \frac{65v^2r^2}{16q_c^{12}} ,$$

$$h_5 = -\frac{5g^2}{2q_c^4} + \frac{931v^2g}{36q_c^8} + \frac{39337v^4}{1458q_c^{12}} ,$$

$$h_5' = -\frac{5g^2}{q_c^4} + \frac{613v^2g}{108q_c^8} + \frac{187633v^4}{2916q_c^{12}} ,$$

$$h_5'' = -\frac{48g^2}{q_c^4} + \frac{55v^2g}{2q_c^8} + \frac{385v^4}{6q_c^{12}} , \tag{13}$$

$$v' = \frac{47vg}{3q_c^4} - \frac{24v^3 - 1385rvg}{108q_c^8} - \frac{13rv^3}{162q_c^{12}} ,$$

$$w = -\frac{99g^2}{2q_c^4} + \frac{20v^2g}{9q_c^8} - \frac{58v^4}{729q_c^{12}} ,$$

whereas g_3 and g_5 have already been given in Eqs. (10) and (11). If the complex amplitudes are written in terms of a modulus and a phase as $A_i = R_i e^{i\phi_i}$, then the sum of the phases, $\phi = \sum_{i=1}^{3} \phi_i$, satisfies

$$\frac{d\phi}{dt} = \lambda_1 \sin\phi + \lambda_2 \sin 2\phi , \tag{14}$$

with

$$\lambda_1 = -6Rv + 9R^3v' , \quad \lambda_2 = 3R^4w , \tag{15}$$

where we have only considered the situation with $R_1 = R_2 = R_3 = R$, in view of the symmetric character of the patterns obtained numerically.

On the other hand the amplitude R obeys

$$\frac{dR}{dt} = rR + 2vR^2\cos\phi - (g_3 + 2h_3)R^3 - \frac{5v'}{2}R^4\cos\phi$$

$$- [(g_5 + 2h_5 + 2h_5' + h_5'') + w\cos 2\phi]R^5 . \tag{16}$$

From (14), the stationary values of the total phase are $\phi = 0$: one has $H0$ hexagons, where the maxima (minima) form a triangular lattice if $v > 0$ $(v < 0)$; $\phi = \pi$: one has $H\pi$ hexagons, where the maxima (minima) form a honeycomb lattice if $v > 0$ $(v < 0)$; $\phi = \phi^* = \cos^{-1}(-\lambda_1/2\lambda_2)$. The linear stability with respect to uniform total phase perturbation $\delta\phi$ is determined by the eigenvalues

$2\lambda_2 + \lambda_1$ for $\phi = 0$,

$2\lambda_2 - \lambda_1$ for $\phi = \pi$,

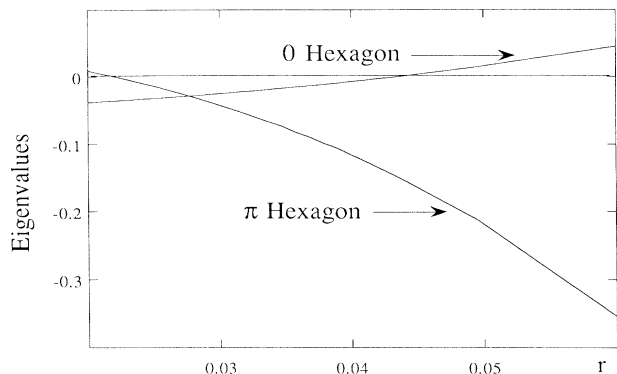$(2\lambda_2 + \lambda_1)(\lambda_1 - 2\lambda_2)/2\lambda_2$ for $\phi = \phi^*$.

FIG. 6. Eigenvalues for the linear stability of the phase of the structures of hexagonal symmetry. The region of bistability of $H\pi$ and $H0$ hexagons, where both eigenvalues are negative, is clearly visible.

The two first eigenvalues are plotted in Fig. 6 for the values of the parameters used in the paper. This diagram shows that there exists a region where the $H0$ and $H\pi$ are both stable with respect to the uniform phase perturbations. Using (16) it may in turn be shown that, in their region of coexistence, the amplitudes of both hexagonal patterns are also stable to uniform perturbations for the chosen values of the parameters. The solution $\phi=\phi^*$ is unstable with respect to total phase perturbations in its domain of existence.

Thus, for $v>0$ (as considered here), we expect, from the amplitude equation analysis, that the $H0$ are the stable patterns for low values of r until they exchange their stability with the $H\pi$ for larger values of the bifurcation parameter after going through a region where both types of hexagons may coexist.

While very heavy, the study of the stability of the patterns of hexagonal symmetry with respect to the formation of stripes leads to the standard result of the hexagonal stripe competition although the stripes here appear subcritically. The only difference is that somewhere in the hexagonal-stripe coexistence region one switches from one type of hexagon to the other. However, as we
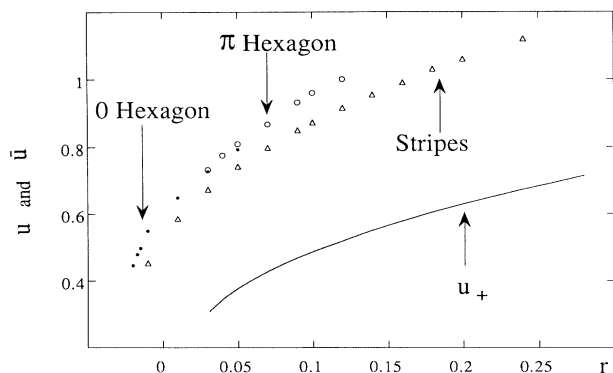
already know, for still higher values of r, the uniform $u_\pm$ states remain the only stable states. Amplitude equations for the other two symmetry-breaking bifurcation points at A and C have not been derived, nor the connection of the branches emanating from these points with those
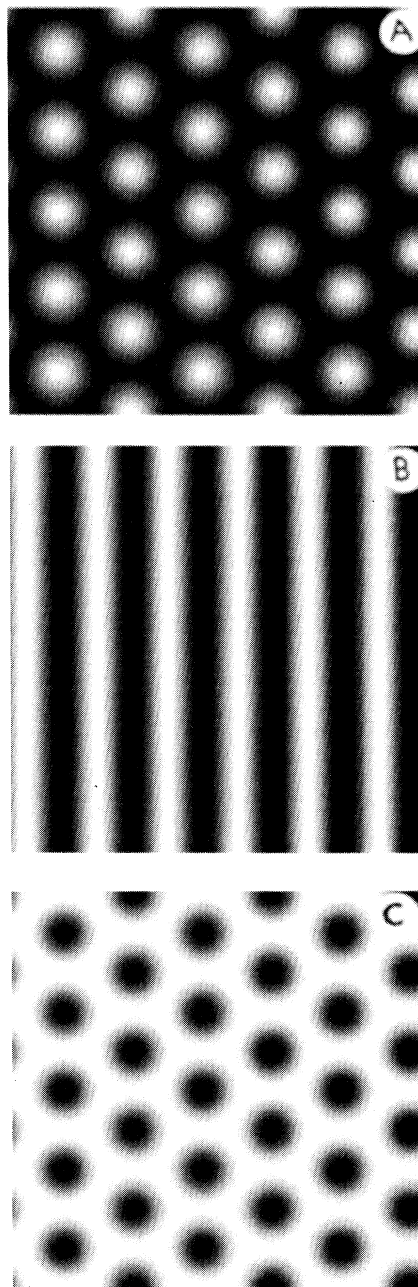

FIG. 7. Bifurcation diagram in two space dimensions obtained from the numerical integration of Eq. (1). The representation is that of Fig. 2.

FIG. 8. Structures for u in Eq. (1). The integration was performed on a square grid of size 64×64 with mixed (see text) boundary conditions. The gray scale corresponds to the concentration between the absolute minimum (black) and maximum (white). (a) $H0$ hexagons for $r=-0.02$; (b) Stripes for $r=-0.01$; (c) $H\pi$ hexagons for $r=0.1$.

studied before.

These results are corroborated by our numerical simulations. In the 2D numerical bifurcation diagram (Fig. 7) the first structure to appear subcritically is indeed of the $H0$ type [Fig. 8(A)]. On increasing r, the $H0$ structure is followed also subcritically (at least for $v = 0.41$) by stripes [Fig. 8(B)]. In the subcritical region ($r < 0$) the system thus exhibits a region of tristability among $H0$, stripes, and the trivial homogeneous steady state ($A = 0$). At still higher values of r (> 0) we observe the predicted reentrant phase of hexagonal symmetry of the $H\pi$ type [Fig. 8(C)], as was already obtained in various chemical models [22–24] as well as in experiments [25]. Here, however, as we have discussed, the two kinds of hexagonal patterns may coexist for set of values of r leading to a high multiplicity of solutions as the stripes, and the uniform u_+ states are also stable for this set of values of the control parameter. The coexistence of the two types of hexagonal patterns seem to have recently been observed experimentally [26] in Rayleigh-Bénard convection in SF_6 near the liquid-gas critical point [27]. As r is increased further, the $H\pi$ become unstable with respect to the formation of stripes or the uniform u_+ states. In the end, the stripes also yield to the uniform u_+ states, which are the only states remaining stable for high r. We have thus obtained qualitative agreement between analytical and numerical results. For other values of the parameters, $v = 0.7$ and $q_c = 1$, we have also obtained stable patterns of square symmetry (see also [28]). Their existence for the parameters used in this paper has not yet been established.

Associated with these phenomena of multistability one observes a large variety of 2D localized structures, some of which are displayed in Fig. 9. Here also the stability of these states heavily relies on domain wall pinning. The
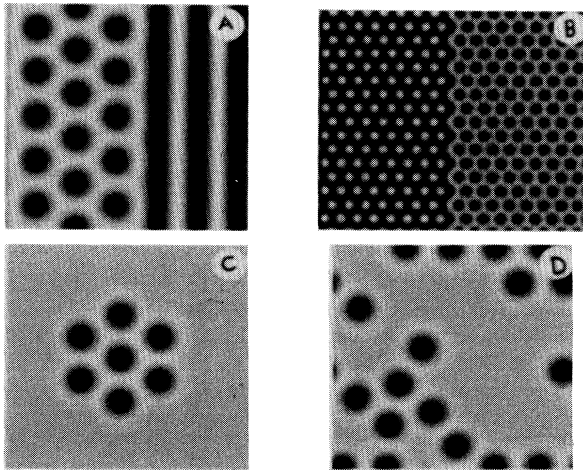
shape of these structures follows from the fact that this pinning is more important when the domain boundary is nearly perpendicular to the wave vectors characterizing the patterns [29].

Our 2D numerical simulations have also produced inhomogeneous states [Fig. 9(C)] that consist of beads of low amplitude embedded in the uniform u_+ state. As the control parameter is decreased the number of spots grows, finally giving rise to the full hexagonal structure ($H\pi$). This spatial disorder has been discussed for large v conditions [28]. Similar inhomogeneous "spotty" states have also been obtained recently in numerical simulations [30] of a variant of the Gray-Scott model [31]. In the latter case, however, the state exhibits a time dependence that is of course absent in our gradient model.

V. RAMPED STRUCTURES

In the case of the chemical structures experimentally obtained in the CIMA reaction the system is kept under control by feeds through the boundaries, and this creates concentration gradients in the system. To study the
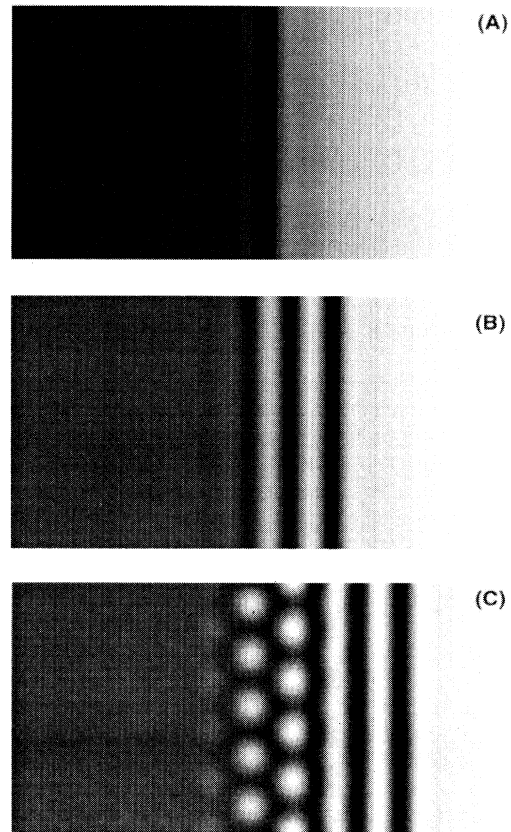

FIG. 9. Localized structures obtained numerically from Eq. (1) at $r = 0.1$, except (b). (a) Stable stationary front between $H\pi$ hexagons and stripes; (b) stable stationary front between $H\pi$ and $H0$ at $r = 0.035$; (c) $H\pi$ hexagonal droplet embedded in the uniform u_+ state; (d) "spotty" state.

FIG. 10. Sequence of structures in the presence of a linear ramp of the control parameter $r = \gamma(2x - 1)$, as the slope γ is progressively decreased. (a) $\gamma = 0.6$; (b) $\gamma = 0.2$; (c) $\gamma = 0.1$.

effect of such concentration profiles on the pattern selection problem presented above for uniform conditions, we have solved numerically Eq. (1) in the presence of a linear ramp of the bifurcation parameter that we now write as $r = \gamma(2x - 1)$.

When the ramp γ is sufficiently steep a single sharp front develops perpendicularly to the gradient. This trivial state corresponds to a rapid switch between the state $u = 0$ and the uniform u_+ state [Fig. 10(A)]. Such a switch could not be present in the previous studies of the effects of the feeding ramps on the chemical pattern selection problem [32], as no bistability between homogeneous steady states existed. On decreasing the ramp two alternating dark and clear stripes develop also parallel to the need boundary [Fig. 10(B)]. A further decrease results in the emergence of an $H0$ pattern that finally breaks the symmetry of the feeding and that spatially coexists with the stripes [Fig. 10(C)]. At this stage we have an unfolding in space of the bifurcation diagram discussed in the preceding section (Fig. 7). Each pattern develops in the region of space where the local value of the bifurcation parameter allows it to be stable. The other hexagonal structure $(H\pi)$ does not occur, as the value of the ramp has suppressed the stability domain of this structure. A similar sequence of structures is observed in the experiments performed [33] in the gel strip reactor when the feeding concentrations of the species along the two boundaries are progressively varied.

VI. CONCLUSIONS

We have shown that, despite its simplicity, the generalized Swift-Hohenberg model exhibits a very rich variety of behaviors that had not been documented before, when the quadratic coupling v is large. Some of these are similar to the observations in experiments in spatial open chemical systems or in numerical studies of more realistic but more complex models. Such are the reentrant hexagonal patterns and their pinning. A feature of this model is that both types of hexagons are able to coexist for a band of values of the control parameter, as seems to have been observed in non-Boussinesq Rayleigh-Bénard experiments. Because of its gradient structure, the model allows for the study of the role of such pinning effects in the origin of the localized structures in absence of non-variational effects [34]. Finally, it may also prove a good candidate for the further studies of the nucleation kinetics of diffusion-driven structures, as well as of the pattern selection problem of ramped 3D Turing structures [35].

ACKNOWLEDGMENTS

[1] M. Cross and P. C. Hohenberg, Rev. Mod. Phys. **65**, 854 (1993).

[2] P. Manneville, *Dissipative Structures and Weak Turbulence* (Academic, Boston, 1990).

[3] G. Nicolis and I. Prigogine, *Self-Organization in Nonequilibrium Systems* (Wiley, New York, 1977).

[4] G. D'Alessandro and W. J. Firth, Phys. Rev. Lett. **66**, 2597 (1991).

[5] J. Swift and P. C. Hohenberg, Phys. Rev. A **15**, 319 (1977).

[6] H. Haken, *Advanced Synergetics* (Springer, Berlin, 1983).

[7] M. Bestehorn and H. Haken, Z. Phys. B **57**, 329 (1984).

[8] S. Ciliberto, P. Coullet, J. Lega, E. Pampaloni, and C. Perez-Garcia, Phys. Rev. Lett. **65**, 2370 (1990).

[9] M. I. Rabinovich, A. L. Fabrikant, and L.S. Tsimring, Usp. Fiz. Nauk **162**, 1 (1992) [Sov. Phys. Usp. **35**, 629 (1992)].

[10] A. Turing, Philos. Trans. R. Soc. London, Ser. B **237**, 37 (1952).

[11] D. Walgraef, G. Dewel, and P. Borckmans, Adv. Chem. Phys. **49**, 311 (1982).

[12] V. Castets, E. Dulos, J. Boissonade, and P. De Kepper, Phys. Rev. Lett. **64**, 2953 (1990).

[13] Q. Ouyang and H. L. Swinney, Nature (London) **352**, 610 (1991).

[14] H. Herrero, C. Perez-Garcia, and M. Bestehorn, Chaos **4**, 15 (1994), and references therein.

[15] H. W. Müller, Phys. Rev. E **49**, 1273 (1994).

[16] P. De Kepper, J. Boissonade, and I. R. Epstein, J. Phys. Chem. **94**, 6525 (1990).

[17] A. C. Newell, T. Passot, and J. Lega, Annu. Rev. Fluid Mech. **25**, 399 (1993).

[18] W. Van Saarloos, Phys. Rev. A **39**, 6367 (1989).

[19] Y. Pomeau, Physica D **23**, 3 (1986).

[20] O. Jensen, V. O. Pannbacker, G. Dewel, and P. Borckmans, Phys. Lett. A **179**, 91 (1993).

[21] K. Binder and A. P. Young, Rev. Mod. Phys. **58**, 801 (1986).

[22] J. Verdasca, A. De Wit, G. Dewel, and P. Borckmans, Phys. Lett. A **168**, 194 (1992).

[23] V. Dufiet and J. Boissonade, Physica A **188**, 158 (1992).

[24] S. Métens, G. Dewel, and P. Borckmans (unpublished).

[25] Q. Ouyang, Z. Noszticzius, and H. L. Swinney, J. Phys. Chem. **96**, 6773 (1992).

[26] M. Assenheimer and V. Steinberg (private communication).

[27] M. Assenheimer and V. Steinberg, Phys. Rev. Lett. **70**, 3888 (1993).

[28] K. A. Gorshkov, L. N. Korzinov, M. I. Rabinovich, and L. S. Tsimring, J. Stat. Phys. **74**, 1033 (1994).

[29] B. Malomed, A. A. Nepomnyashchy, and M. I. Tribelsky, Phys. Rev. A **42**, 7244 (1990).

[30] J. E. Pearson, Science **261**, 189 (1993).

[31] P. Gray and S.K. Scott, Chem. Eng. Sci. **38**, 29 (1983).

[32] P. Borckmans, A. De Wit, and G. Dewel, Physica A **188**, 137 (1992).

[33] P. De Kepper, V. Castets, E. Dulos, and J. Boissonade, Physica D **49**, 161 (1991).

[34] O. Thual and S. Fauve, J. Phys. (Paris) **49**, 1829 (1988).

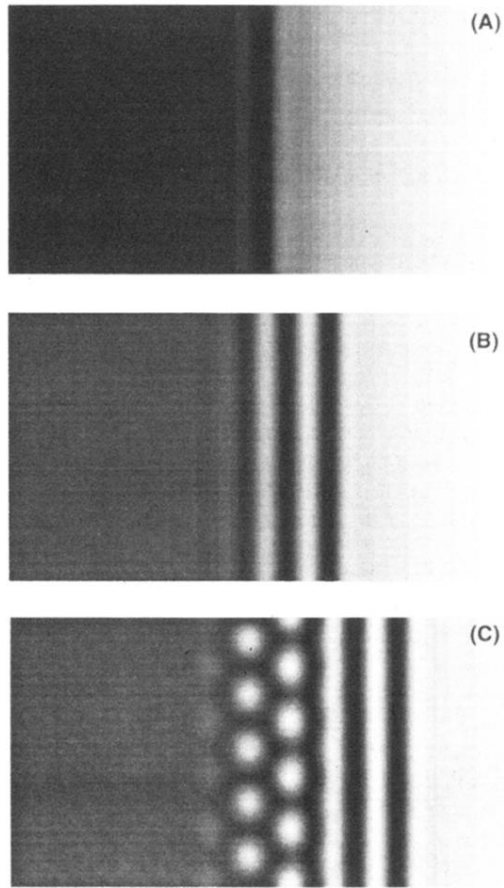[35] A. De Wit, G. Dewel, P. Borckmans, and D. Walgraef, Physica D **61**, 289 (1992).

FIG. 10. Sequence of structures in the presence of a linear ramp of the control parameter $r = \gamma(2x - 1)$, as the slope γ is progressively decreased. (a) $\gamma = 0.6$; (b) $\gamma = 0.2$; (c) $\gamma = 0.1$.
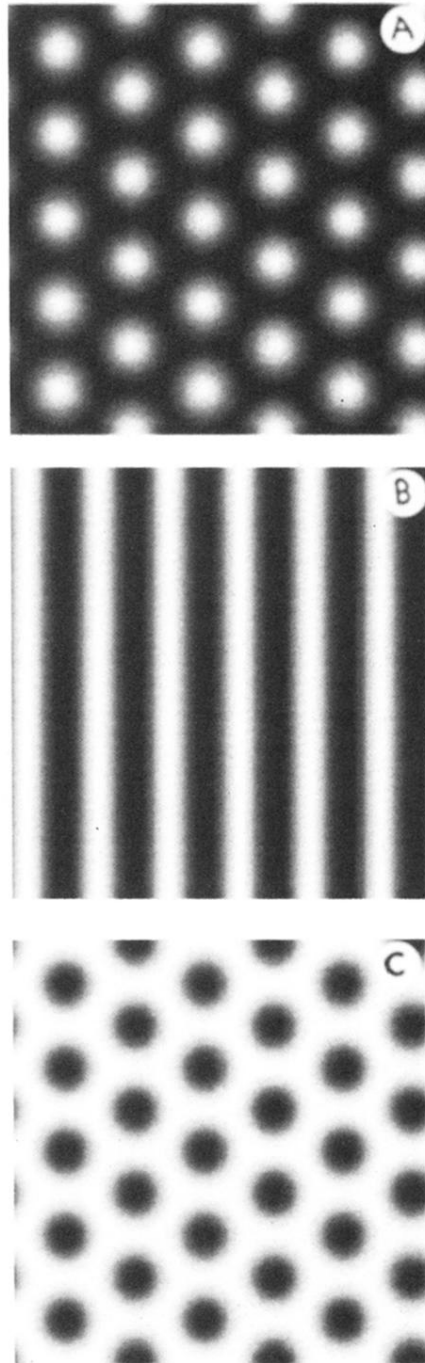
FIG. 8. Structures for u in Eq. (1). The integration was performed on a square grid of size 64×64 with mixed (see text) boundary conditions. The gray scale corresponds to the concentration between the absolute minimum (black) and maximum (white). (a) $H0$ hexagons for $r = -0.02$; (b) Stripes for $r = -0.01$; (c) $H\pi$ hexagons for $r = 0.1$.
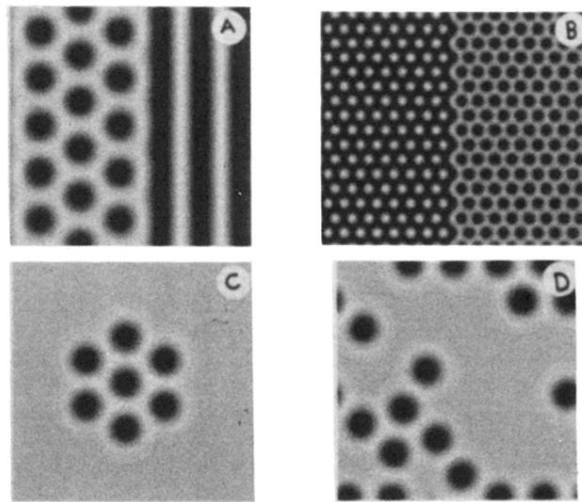
FIG. 9. Localized structures obtained numerically from Eq. (1) at $r = 0.1$, except (b). (a) Stable stationary front between $H\pi$ hexagons and stripes; (b) stable stationary front between $H\pi$ and $H0$ at $r = 0.035$; (c) $H\pi$ hexagonal droplet embedded in the uniform u_+ state; (d) "spotty" state.